Raman-Ramsey resonances in atomic vapor cells: Rabi pulling and optical-density effects

Salvatore Micalizio and Aldo Godone

INRIM, Istituto Nazionale di Ricerca Metrologica, Strada delle Cacce 91, 10135 Torino, Italy

Raman-Ramsey interference has proved a very effective technique to implement compact and high performing vapor cell frequency standards. In this paper, we theoretically characterize Raman-Ramsey resonances in an optically thick atomic vapor. Specifically, some parameters of interest for frequency standards applications, like contrast and linewidth of the central Raman-Ramsey fringe, are evaluated at different temperatures for [133]Cs and [87]Rb vapor cells with buffer gas. Density narrowing and broadening effects are described and explained in terms of a three-level theory where laser field propagation through the atomic medium is taken into account. Also, we investigate light shift both in low and high atomic density regimes. Light shift, which potentially degrades the medium- to long-term stability of Raman-Ramsey clocks, is composed of two contributions. The first is a pulling effect exerted by the wide Rabi profile enclosing the interference pattern on the central Raman-Ramsey fringe. The second light-shift term is strictly related to the detection time. Calculations derived from our model well describe already existing experimental results and new behaviors are predicted.

I. INTRODUCTION

Coherent population trapping (CPT) is a phenomenon where optical excitation is done by means of two phase-coherent laser fields coupling two atomic ground-state levels to a common excited state (Λ interaction scheme) [1,2]. At resonance, a quantum interference takes place, resulting in the absence of light absorption by the atoms. Specifically, the atoms are pumped in a nonabsorbing coherent super-position of the ground-state levels and the atomic medium becomes transparent to the applied optical radiation. Due to the resonant nature of the phenomenon, CPT has been used in several applications, including frequency standards [3,4] and magnetometry [5–7]. It is also exploited in the study of light-matter interaction, like slow light experiments [8–10] and velocity-selective laser cooling [11].

First observations of CPT resonances as clock references were done on atomic beams [12–14]. However, it is with vapor cell devices that CPT has been extensively applied to frequency metrology [15]. In the last decade, CPT clocks with high-frequency stability performances have been developed by several groups using Rb or Cs vapors in a cell with buffer gas [16–23]. Also, thanks to the use of microelectromechanical systems, CPT has allowed the implementation of chip-scale atomic devices [24–26]. More recently, a CPT clock based on cold atoms has been demonstrated [27].

Compared to a traditional double-resonance approach [28,29], CPT in principle offers some advantages. First, there is no need of any microwave cavity to excite the microwave clock transition: in some sense, the microwave field is carried by the bichromatic optical field itself. This results in a more compact physics package and all the effects related to the cavity (through cavity pulling) disappear. In addition, the Λ interaction allows a first-order light-shift compensation [30–35], with some benefit for the medium-term stability of the clock. However, CPT clock resonances observed in the continuous regime suffer for power broadening and are not immune to laser intensity and/or frequency fluctuations. The pulsed approach proved one of the most effective techniques to mitigate these issues and consequently improve the stability performances of CPT vapor cell clocks. The main idea is to probe the clock transition in a Ramsey-like experiment. The atomic sample experiences a first Λ pulse of duration τ_1 which prepares the atoms in the dark state. Then the atoms freely evolve for a time T limited by the relaxation phenomena taking place inside the cell, mainly spin-exchange, buffer gas, and cell wall collisions. Finally, a second Λ pulse of duration τ_2 probes the phase of the dark state. This scheme allows the detection of the so-called Raman-Ramsey interference fringes [36]: the central fringe is a narrow resonance, the linewidth $\Delta\nu_{1/2}$ of which is in principle related to the observation time only ($\Delta\nu_{1/2} = 1/2T$) and free of any power broadening. In addition, the atoms make the clock transition mainly in the dark, when the laser is off, and a greatly reduced sensitivity to laser instabilities is expected. Actually, this ideal situation is not fully observed in experiments. First, the shape of the central Ramsey fringe appears slightly asymmetric and the relation $1/2T$ usually adopted to estimate its linewidth does not always fit the experimental data. Moreover, the frequency stability of CPT clocks (Allan deviation) is still affected by laser-induced frequency fluctuations and only very recently Allan deviations in the 10^{-15} range have been measured for integration times around 10 000 s, thanks to autobalanced Ramsey techniques [37].

The purpose of this paper is to theoretically discuss a few phenomena that contribute to define the laser-induced shift of the clock transition, the shape of Raman-Ramsey fringes, and the contrast and the linewidth of the central fringe in pulsed CPT.

We first demonstrate that the detection process gives rise to a light-shift term which is linear in the detection time and in the laser pumping rate. It is an unavoidable shift inherent to

the detection of the clock signal and can be minimized only by reducing the detection time itself.

We then describe a Rabi pulling-like effect through which laser instabilities are transferred to the clock transition. Specifically, we will show that the envelope of Raman-Ramsey fringes turns out to be affected by off-resonant light shift which produces a pulling of the central interference fringe. We point out that this Rabi pulling effect does not originate from neighboring transitions as that observed in Cs beam tubes or fountains. Rather, it is due to the fact that the clock resonance (Ramsey fringe) is embedded in a larger and shifted profile (Rabi profile) exerting a dragging on the clock frequency, a situation similar, for example, to the cavity pulling.

The last effect we discuss is the role played by atomic density. We will show that for an optically thick medium (as is any actual vapor cell arrangement) the linewidth significantly differs from the well-known relation $1/2T$ and depends on the vapor temperature. Two regimes can be distinguished as the atomic density is increased: a density narrowing of the linewidth followed by a density broadening when the vapor temperature, and then the atomic density, is increased above a certain value. We will explain the behavior of the pulsed CPT central fringe contrast versus the atomic density, a behavior observed in experiments but, to our knowledge, not yet fully explained in the frame of a theoretical model. We will also study the linewidth dependence on the laser intensity and we will show that an increase of the laser intensity does not always produce a broadening.

The paper is organized as follows. Section II is devoted to CPT in an optically thin atomic medium. We first shortly review the main properties of CPT resonances observed in a cell with buffer gas in continuous operation. Even if the results of this subsection are known and well established in the literature, this first paragraph is preparatory to the following sections and allows us to present the formalism we adopt throughout the paper.

We then describe the pulsed approach, with particular attention to the light shift induced by the Rabi profile on the Raman-Ramsey central fringe.

In Sec. III, the previous analysis is extended to an optically thick medium. Solutions of the Maxwell-Bloch equations for vapor cell arrangements using either ^{133}Cs or ^{87}Rb in buffer gas are discussed. We show that our theory is able to describe the behavior of linewidth and contrast of Raman-Ramsey resonances versus the vapor temperature and laser intensity, as observed in [38,39].

Possible impact on clock implementation and conclusions are reported in Sec. IV.
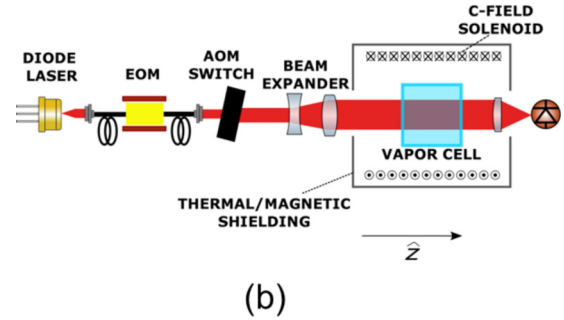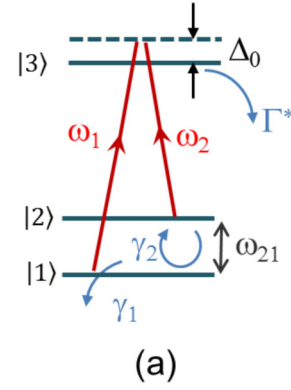

FIG. 1. (a) Three-level system considered in the theory. Γ^* is the excited-state relaxation rate; γ_1 and γ_2 are the relaxation rates for ground-state population and coherence, respectively; Δ_0 is the laser detuning; ω_{21} is the ground-state (angular) Bohr frequency. (b) Setup scheme of the principle: the electro-optic modulator (EOM) generates the two phase-coherent laser frequencies ω_1 and ω_2 starting from the D_1 laser carrier; the acousto-optic modulator (AOM) is used to pulse the laser.

II. THIN ATOMIC MEDIUM

A. CPT resonance in continuous operation

We consider a three-level atomic system where two ground-state sublevels are coupled to a common excited state via two phase coherent laser fields. The theoretical model to describe this system can be found in several works in the literature; we specifically refer to the framework developed for the CPT maser [16].

Our analysis is based on the closed three-level system and on the conceptual arrangement sketched in Fig. 1.

The atoms are diluted in a cell also containing a buffer gas and interact with a bichromatic laser field propagating along the $\hat{z}$ axis and tuned to D_1 transition. Along the same axis, a

quantization magnetic field is applied to the atomic sample. The density-matrix equations governing the system can be written as

$$\dot{\rho}_{33} + \Gamma^* \rho_{33} = \frac{1}{1+\delta_0^2} \left[\frac{\omega_{R1}^2 + \omega_{R2}^2}{2\Gamma^*} + \Delta \left(\frac{\omega_{R1}^2 - \omega_{R2}^2}{2\Gamma^*} \right) + \frac{2\omega_{R1}\omega_{R2}}{\Gamma^*} \delta_{12}^r \right],$$

$$\dot{\Delta} + \left(\gamma_1 + \frac{\omega_{R1}^2 + \omega_{R2}^2}{2\Gamma^*(1+\delta_0^2)} \right) \Delta = \frac{1}{1+\delta_0^2} \left[\frac{\omega_{R1}^2 - \omega_{R2}^2}{2\Gamma^*} + \frac{2\delta_0\omega_{R1}\omega_{R2}}{\Gamma^*} \delta_{12}^i \right],$$

$$\dot{\delta}_{12} + \left[\gamma_2 + \frac{\omega_{R1}^2 + \omega_{R2}^2}{2\Gamma^*(1+\delta_0^2)} + i(\Omega_\mu - \Delta\omega_{LS}) \right] \delta_{12} = -\frac{\omega_{R1}\omega_{R2}}{2\Gamma^*(1+\delta_0^2)} - i\frac{\omega_{R1}\omega_{R2}}{2\Gamma^*(1+\delta_0^2)} \delta_0\Delta, \qquad (1)$$

where ρ_{33} is the the atomic population of the excited state, $\Delta \equiv \rho_{22} - \rho_{11}$ is the ground-state population difference, and δ_{12} ($\delta_{12} \equiv \delta_{12}^r + i\delta_{12}^i$) is the coherence excited between the ground-state sublevels; γ_1 and γ_2 are the relaxation rates for the ground-state population difference and coherence, respectively.

We consider the excited-state relaxation rate Γ^* as resulting from the convolution of collision broadening (atom-buffer gas) and Doppler broadening. Rigorously, Doppler broadening should be taken into account by averaging the density-matrix elements over the Maxwell velocity distribution. However, for buffer-gas pressures typically used in experiments, we adopt the approximation of homogeneous broadening since the width Γ_{BG} equals or even exceeds Γ_D, where Γ_{BG} and Γ_D are the homogeneous broadening due to buffer gas collisions and to the Doppler broadening, respectively. The residual Doppler broadening is taken into account in the convoluted relaxation rate evaluated according to the relation reported in [40], $\Gamma^* = \frac{1}{2}[\Gamma_{\mathrm{BG}} + \sqrt{\Gamma_{\mathrm{BG}}^2 + 4\Gamma_D^2}]$.

Previous equations are obtained under the rotating-wave approximation and assuming $\omega_{R1,2} \ll \Gamma^*$, where ω_R is the optical Rabi frequency and Ω_μ is the two-photon (Raman) microwave detuning; Δ_0 is the detuning of the laser field from the optical transition and $\delta_0 \equiv 2\Delta_0/\Gamma^*$.

The quantity

$$\Delta\omega_{LS} \equiv \frac{\omega_{R2}^2 - \omega_{R1}^2}{2\Gamma^*}\frac{\delta_0}{1 + \delta_0^2} + \frac{\omega_{R1}^2 + \omega_{R2}^2}{4\omega_{21}} \tag{2}$$

accounts for the light shift and is composed of a dispersive Lorentzian term versus the laser detuning and of a term solely depending on the laser intensity. In many experimental arrangements, the Λ transition on the D_1 line is driven by the two first-order sidebands created by an electro-optical modulator and this guarantees that $\omega_{R1} = \omega_{R2} \equiv \omega_R$; this hypothesis is supposed to hold throughout the paper. The set of equations in the typical operating condition ($\Delta_0, \Gamma^* \ll \omega_{21}$, $\delta_0 \ll 1$) becomes

$$\dot{\Delta} + (\gamma_1 + 2\Gamma_p)\Delta = 4\Gamma_p\delta_0\delta_{12}^i,$$
$$\dot{\delta}_{12} + \left[\gamma_2 + 2\Gamma_p + i\left(\Omega_\mu - \omega_R^2/2\omega_{21}\right)\right]\delta_{12} = -\Gamma_p - i\Gamma_p\delta_0\Delta,$$
$$\rho_{33} = \left(\frac{\omega_R}{\Gamma^*}\right)^2\left\{1 + 2\delta_{12}^r\right\}, \tag{3}$$

where we defined the (transversal) pumping rate:

$$\Gamma_p = \frac{\omega_R^2}{2\Gamma^*}. \tag{4}$$

In the continuous case, the equations can be solved in steady-state conditions. Specifically, for an optically thin medium the resonant behavior of the CPT phenomenon is captured by the fluorescence spectrum P_{fl} that is proportional to the population of the excited state ρ_{33}. It turns out that

$$P_{\mathrm{fl}} \propto \rho_{33} = \left(\frac{\omega_R}{\Gamma^*}\right)^2\left\{1 - \frac{2\Gamma_p}{\Gamma'}\frac{\Gamma'^2 + 4\Gamma_p^2\delta_0^2}{\Gamma'^2 + 4\Gamma_p^2\delta_0^2 + \left(\Omega_\mu - \omega_R^2/2\omega_{21}\right)^2}\right\}, \tag{5}$$

where we defined

$$\Gamma' = \gamma_2 + 2\Gamma_p. \tag{6}$$

The CPT resonance turns out to be a Lorentzian slightly broadened by the term proportional to δ_0 (negligible in most applications) and shifted by the intensity light-shift term. Therefore, as far as the conditions $\omega_{R1} = \omega_{R2}$ and $\delta_0 \ll 1$ are satisfied, there is not any frequency modulation-to-frequency modulation (FM-FM) conversion from the laser to the atomic resonance.

B. CPT resonances in pulsed operation: Rabi pulling and detection light shift

To describe CPT resonances in pulsed operation, Eqs. (3) need to be solved in the transient regime. Specifically, we are interested in implementing a Raman-Ramsey interaction scheme where a first Λ pulse of duration τ_1 pumps the atoms into the dark state. The atoms are then let free to evolve for a time T and finally the accumulated phase between the dark state and the local oscillator is probed through a second Λ pulse of duration τ_2 (see the time sequence in Fig. 2).

We note that the equations for the coherence and the population are coupled but linear, thereby we can apply the technique of Laplace transform to solve them. Moreover, since the end of each phase gives the initial condition for the subsequent phase, it is convenient to introduce a matrix formalism where atomic coherence and population are arranged in a vector (Bloch vector) [41,42]:

$$\mathbf{R}(t) = \begin{pmatrix} \delta_{12}^r(t) \\ \delta_{12}^i(t) \\ \Delta(t) \end{pmatrix}. \tag{7}$$

We consider the first Λ pulse under the assumption that initially the atomic sample does not have any coherence ($\delta_{12} = 0$) and the atomic population is equally distributed among the two ground-state sublevels ($\rho_{11} = \rho_{22}$, i.e., $\Delta = 0$). Solving Eqs. (3), we find for the Bloch vector $\mathbf{R}(\tau_1)$ the
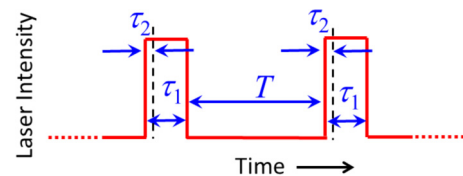

FIG. 2. Time sequence of the Raman-Ramsey pulses: τ_1 is the duration of the Λ pulse, T is the free evolution time, and τ_2 is the detection time.

following components:

$$\mathbf{R}(\tau_1) = \begin{pmatrix} -\dfrac{\Gamma_p\Gamma'}{\Gamma'^2 + \Omega_\mu'^2} + \dfrac{e^{-\Gamma'\tau_1}\Gamma_p(\Gamma'\cos\Omega_\mu'\tau_1 - \Omega_\mu'\sin\Omega_\mu'\tau_1)}{\Gamma'^2 + \Omega_\mu'^2} \\[4mm] \dfrac{\Gamma_p\Omega_\mu'}{\Gamma'^2 + \Omega_\mu'^2} - \dfrac{e^{-\Gamma'\tau_1}\Gamma_p(\Omega_\mu'\cos\Omega_\mu'\tau_1 + \Gamma'\sin\Omega_\mu'\tau_1)}{\Gamma'^2 + \Omega_\mu'^2} \\[4mm] \dfrac{4\Gamma_p^2\delta_0\Omega_\mu'}{\Gamma'(\Gamma'^2 + \Omega_\mu'^2)} - \dfrac{4e^{-\Gamma'\tau_1}\Gamma_p^2\delta_0}{\Gamma'\Omega_\mu'} + \dfrac{4\Gamma_p^2\delta_0 e^{-\Gamma'\tau_1}}{\Omega_\mu'(\Gamma'^2 + \Omega_\mu'^2)}(\Gamma'\cos\Omega_\mu'\tau_1 - \Omega_\mu'\sin\Omega_\mu'\tau_1) \end{pmatrix}, \tag{8}$$

where we defined $\Omega_\mu' \equiv \Omega_\mu - \frac{\omega_R^2}{2\omega_{21}}$.

The solutions are controlled by the exponential term $e^{-\Gamma'\tau_1}$; in particular, for $\Gamma'\tau_1 \gg 1$ the solutions reproduce the steady-state behavior: the atomic system is pumped in the dark state and the Bloch vector simplifies to

$$\mathbf{R}(\tau_1 \gg 1/\Gamma') = \begin{pmatrix} -\frac{\Gamma_p\Gamma'}{\Gamma'^2 + \Omega_\mu'^2} \\[3mm] \frac{\Gamma_p\Omega_\mu'}{\Gamma'^2 + \Omega_\mu'^2} \\[3mm] \frac{4\Gamma_p^2\delta_0\Omega_\mu'}{\Gamma'(\Gamma'^2 + \Omega_\mu'^2)} \end{pmatrix}. \tag{9}$$

As expressed in Eq. (9), the Bloch vector reproduces a well-known result of CPT theory: whatever the initial conditions, the CPT phenomenon drives the atoms in the dark state provided the Λ pulse area (intensity times duration) is sufficiently large.

In the following phase, the Bloch vector evolves for a time T according to the free evolution matrix $\hat{M}_D(T)$:

$$\hat{M}_D(T) = \begin{pmatrix} e^{-\gamma_2 T}\cos\Omega_\mu T & e^{-\gamma_2 T}\sin\Omega_\mu T & 0 \\ -e^{-\gamma_2 T}\sin\Omega_\mu T & e^{-\gamma_2 T}\cos\Omega_\mu T & 0 \\ 0 & 0 & e^{-\gamma_1 T} \end{pmatrix}, \tag{10}$$

so that we have

$$\mathbf{R}(T + \tau_1) = \hat{M}_D(T) \cdot \mathbf{R}(\tau_1). \tag{11}$$

Note that during the free evolution the laser is off, consequently the atomic phase evolves at an angular frequency Ω_μ, whereas during the first Λ pulse the phase is affected by the off-resonant light shift term $\omega_R^2/2\omega_{21}$.

Equation (11) yields

$$\mathbf{R}(T + \tau_1) = \begin{pmatrix} -\frac{\Gamma_p}{\Gamma'^2 + \Omega_\mu'^2}[\Gamma'\cos\Omega_\mu T - \Omega_\mu'\sin\Omega_\mu T]e^{-\gamma_2 T} \\[3mm] \frac{\Gamma_p}{\Gamma'^2 + \Omega_\mu'^2}[\Gamma'\sin\Omega_\mu T + \Omega_\mu'\cos\Omega_\mu T]e^{-\gamma_2 T} \\[3mm] \frac{4\Gamma_p^2}{\Gamma'}\frac{\delta_0\Omega_\mu'}{\Gamma'^2 + \Omega_\mu'^2}e^{-\gamma_1 T} \end{pmatrix}. \tag{12}$$

The evolution of the Bloch vector during the query Λ pulse of duration τ_2 can be obtained by solving Eqs. (3) with $\delta_{12}^r(T + \tau_1)$, $\delta_{12}^i(T + \tau_1)$ and $\Delta(T + \tau_1)$ as initial conditions. In the general case of $\delta_0 \neq 0$ that solution is rather involute. However, in the experiments the laser is usually frequency locked with zero or negligible detuning, and, since in the previous section we have seen that for $\delta_0 \ll 1$ there is not significant FM-FM conversion, in the following we will consider $\delta_0 = 0$. The only quantity of interest is the real part of the coherence [see the third equation of Eqs. (3)] that turns out to be

$$\delta_{12}^r(\tau_1 + T + \tau_2) = -\frac{\Gamma_p\Gamma'}{\Gamma'^2 + \Omega_\mu'^2} - \frac{\Gamma_p e^{-\Gamma'\tau_2}}{\Gamma'^2 + \Omega_\mu'^2}[(\Gamma'\cos\Omega_\mu T - \Omega_\mu'\sin\Omega_\mu T)e^{-\gamma_2 T} - \Gamma']\cos\Omega_\mu'\tau_2$$

$$+ \frac{\Gamma_p e^{-\Gamma'\tau_2}}{\Gamma'^2 + \Omega_\mu'^2}[(\Gamma'\sin\Omega_\mu T - \Omega_\mu'\cos\Omega_\mu T)e^{-\gamma_2 T} - \Omega_\mu']\sin\Omega_\mu'\tau_2. \tag{13}$$

From the previous equation, it is possible to numerically evaluate two observables of interest for frequency standards applications, the linewidth and the shift of the central Ramsey fringe versus the laser pumping rate.

Figure 3 shows that the linewidth quickly approaches the expected value $1/2T$ and eventually overcomes it. As already observed in [38], the pulsed regime allows us to significantly reduce the linewidth and its dependence on the laser power compared to the continuous case. However, power broadening

still affects the resonance linewidth through the length of the detection process.

In Fig. 4 we report the calculated frequency shifts of the central Ramsey fringe versus the laser pumping rate for different values of the detection times. In order to give more physical insight into the effects contributing to the shift, it is useful to examine Eq. (13) in two conditions. First, since we are interested in the central fringe, we consider the limit $\Omega_\mu' \ll \Gamma'$. In addition, we suppose $\tau_2 \ll T$, a condition

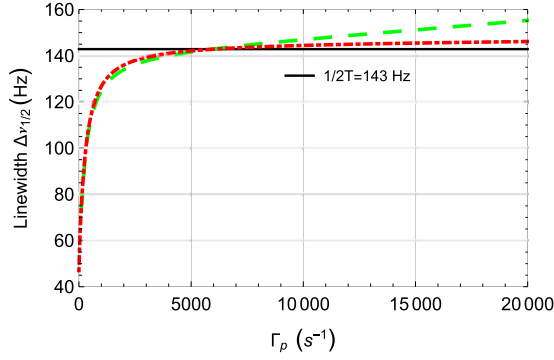FIG. 3. Calculated linewidth of the central Ramsey fringe vs Γ_p; $\gamma_2 = 300 \text{ s}^{-1}$; $T = 3.5$ ms; dash-dotted line, $\tau_2 = 10$ μs; dashed line, $\tau_2 = 100$ μs.

generally satisfied in the experiments, so that Eq. (13) reduces to

$$\delta_{12}^r(\tau_1 + T + \tau_2) \approx -\frac{\Gamma_p}{\Gamma'} e^{-\gamma_2 T - \Gamma' \tau_2} \cos\left[\Omega_\mu T - \frac{\Gamma^* \Gamma_p}{\omega_{21}} \tau_2\right]$$
$$+ \frac{\Gamma_p}{\Gamma'}(e^{-\Gamma' \tau_2} - 1), \qquad (14)$$

which shows that the detection time plays a role also in affecting the central fringe frequency. Specifically, a linear light shift $\Delta\omega_{\text{DT}}$ related to the detection time (DT) τ_2 arises:

$$\frac{\Delta\omega_{\text{DT}}}{\omega_{21}} \approx \frac{\Gamma^* \Gamma_p}{\omega_{21}^2} \frac{\tau_2}{T}. \qquad (15)$$

This detection-time-dependent light shift results in a significant amplitude-to-frequency conversion; for the values used in Fig. 4 (taking, for example, the intermediate curve, $\tau_2 = 50$ μs), it is of the order of 2×10^{-12}/%.

Another source of shift can be identified by noticing that the Rabi profile is centered at $\Omega_\mu' = 0$, whereas the Ramsey fringes are centered at $\Omega_\mu = 0$. Therefore, in the more general case, the role of the Rabi envelope cannot be disregarded since it induces a shift of the central fringe. To investigate this pulling effect of the Rabi profile on the central Ramsey fringe,
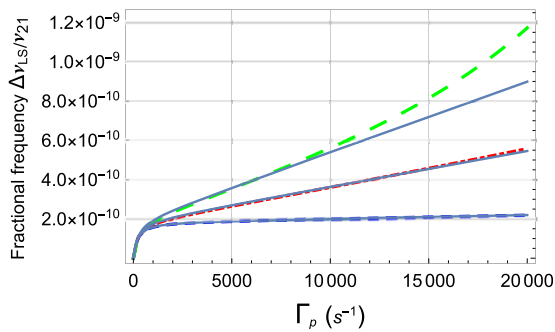

FIG. 4. Calculated light shift of the central Ramsey fringe vs Γ_p; $\gamma_2 = 300 \text{ s}^{-1}$; $T = 3.5$ ms; $\Gamma^* = 2\pi \times 684$ MHz; small-dashed line, $\tau_2 = 5$ μs; dash-dotted line, $\tau_2 = 50$ μs; large-dashed line, $\tau_2 = 100$ μs. For each curve, the approximated expression of the shift given by Eq. (19) has been superimposed to the numerically calculated behavior.

we specify Eq. (13) in the limit $\tau_2 \to 0$:

$$\delta_{12}^r(\tau_1 + T + \tau_2)$$
$$\approx -\frac{\Gamma_p}{\Gamma'^2 + \Omega_\mu'^2}[(\Gamma' \cos\Omega_\mu T - \Omega_\mu' \sin\Omega_\mu T)e^{-\gamma_2 T}]. \quad (16)$$

The shift can be calculated by deriving Eq. (16) with respect to Ω_μ; neglecting second-order terms in Ω_μ, we find a Rabi pulling (RP) induced light shift given by

$$\frac{\Delta\omega_{\text{RP}}}{\omega_{21}} \approx \frac{\Gamma^*}{\omega_{21}^2 T} \frac{\Gamma_p}{\gamma_2 + 2\Gamma_p}. \qquad (17)$$

This light shift is responsible for an amplitude-to-frequency conversion given by

$$\frac{\partial(\Delta\omega_{\text{RP}}/\omega_{21})}{\partial\Gamma_p/\Gamma_p} \approx \frac{\Gamma^*}{\omega_{21}^2 T} \frac{\gamma_2 \Gamma_p}{(\gamma_2 + 2\Gamma_p)^2}. \qquad (18)$$

For common values of the experimental parameters, the previous sensitivity coefficient is 1×10^{-13}/% and reduces by increasing the laser power. This behavior is simply explained by considering that the Rabi profile linewidth is $2\Gamma'$ and not $1/\tau_1$, as in the common Ramsey interaction scheme. Therefore, the Rabi profile broadens with Γ_p and its pulling effect on the central Ramsey fringes reduces accordingly.

Taking into account both the effects, the central Ramsey fringe turns out to be shifted by two light-shift terms of different physical origins:

$$\frac{\Delta\omega_{LS}}{\omega_{21}} = \frac{\Delta\omega_{\text{DT}}}{\omega_{21}} + \frac{\Delta\omega_{\text{RP}}}{\omega_{21}} = \frac{\Gamma^* \Gamma_p}{\omega_{21}^2 T}\left(\tau_2 + \frac{1}{\gamma_2 + 2\Gamma_p}\right). \quad (19)$$

The continuous curves superimposed onto the dashed lines of Fig. 4 represent Eq. (19) in the same conditions used to numerically evaluate the shifts. For small Γ_p, the Rabi pulling effect prevails, while for large Γ_p the shift related to the detection time becomes dominant. Increasing the detection times, nonlinear terms cannot be neglected and Eq. (19) fails to predict the correct behavior for large Γ_p (see the curve corresponding to $\tau_2 = 100$ μs in the figure).

The results obtained so far are valid in the ideal case of a thin optical medium; we will see in the next section how this scenario is modified as the atomic density is increased.

III. THICK ATOMIC MEDIUM

A. Theory

To extend the previous analysis to a thick atomic vapor, we have to consider Maxwell's equations for the laser fields propagating in the atomic medium. Due to absorption, the laser field amplitude is now a function of the position inside the cell.

In the limit of the slowly varying approximation for the optical Rabi frequencies ω_{R1} and ω_{R2} and assuming a linear response of the atomic vapor, the rate equations describing the interaction of the atomic sample with the Λ pulse

become [16]

$$\dot{\Delta} + \left(\gamma_1 + \frac{\omega_{R1}^2 + \omega_{R2}^2}{2\Gamma^*}\right)\Delta = \frac{\omega_{R1}^2 - \omega_{R2}^2}{2\Gamma^*},$$

$$\dot{\delta}_{12} + \left[\gamma_2 + \frac{\omega_{R1}^2 + \omega_{R2}^2}{2\Gamma^*} + i\left(\Omega_\mu - \frac{\omega_{R1}^2 + \omega_{R2}^2}{4\omega_{21}}\right)\right]\delta_{12}$$

$$= -\frac{\omega_{R1}\omega_{R2}}{2\Gamma^*},$$

$$\frac{\partial \omega_{R1}}{\partial z} = -\alpha\left[\frac{\omega_{R1}}{2\Gamma^*}(1-\Delta) + \frac{\omega_{R2}}{\Gamma^*}\delta_{12}^r\right],$$

$$\frac{\partial \omega_{R2}}{\partial z} = -\alpha\left[\frac{\omega_{R2}}{2\Gamma^*}(1+\Delta) + \frac{\omega_{R1}}{\Gamma^*}\delta_{12}^r\right]. \tag{20}$$

In Eqs. (20), α is the absorption coefficient:

$$\alpha = \frac{\omega_L d_e^2}{\epsilon_0 \hbar c} n, \tag{21}$$

where ω_L and d_e are the (angular) frequency and the dipole moment of the D_1 line, respectively; n is the atomic density, ϵ_0 is the vacuum permittivity, $\hbar$ is the (reduced) Planck constant, and c is the speed of light in vacuum.

We neglected the terms proportional to the laser detuning δ_0, since we suppose the laser is frequency stabilized with a negligible detuning, and in the previous section we have seen that when $\delta_0 \ll 1$ neither FM-FM nor frequency modulation-to-amplitude modulation (FM-AM) conversions affect the clock signal.

Equations (20) can be further simplified for the D_1 line we consider in this paper: if at the entrance of the cell we have $\omega_{R1}(z=0) = \omega_{R2}(z=0)$, then a general solution of Eq. (20) is $\omega_{R1}(z) = \omega_{R2}(z) \equiv \omega_R(z)$ for every z and Δ identically equal to zero everywhere inside the cell and at any time. Of course, this result is valid for the three-level model considered in this paper that neglects the Zeeman structure both in the ground and in the excited states.

The ground-state Zeeman structure is usually resolved by a static quantization magnetic field. However, to develop a theory closer to experiments it is important to take into account the Zeeman structure, at least in a phenomenological way. The motivation is that all the ground-state atoms contribute to the absorption process, but only a part of them is involved in the CPT phenomenon and generates the clock signal we are interested in. As already done in [43], we then introduce in the equations a parameter $\alpha' = \frac{\alpha}{2I+1}$ (I being the nuclear spin) which accounts for the fraction of ground-state atoms effectively excited by CPT and detected in the clock operation. In other words, α' gives the weight of the coherent process induced by CPT with respect to light absorption due to all the atoms in the ground-state manifold.

Equations (20) can be finally written in terms of the pumping rate Γ_p as

$$\dot{\delta}_{12} + \left[\gamma_2 + 2\Gamma_p + i\left(\Omega_\mu - \frac{\Gamma^*\Gamma_p}{\omega_{21}}\right)\right]\delta_{12} = -\Gamma_p,$$

$$\frac{\partial \Gamma_p}{\partial z} = -\frac{\Gamma_p}{\Gamma^*}[\alpha + 2\alpha'\delta_{12}^r], \tag{22}$$

and they can be solved either for ^{133}Cs ($I = 7/2$) or ^{87}Rb ($I = 3/2$) or any other alkali-metal atom.

If Eqs. (22) are specified for the first pumping Λ pulse, the solution for δ_{12} is formally the same as that reported by Eq. (9), but now the coherence also depends on z through Γ_p [we remind the reader that Γ' is also a function of z, see Eq. (6)]. Notably, we do not assume as in the previous section that the Λ pulse pumps all the atoms in the dark state. Since absorption occurs in the cell, this is in general not true, especially at the end of the cell where, for high atomic densities, the laser might be strongly attenuated and the inequality $\Gamma'\tau_1 \gg 1$ is not satisfied for every z.

Thereby, at the end of τ_1 we have

$$\delta_{12}^r(z, \tau_1) = -\frac{\Gamma_p\Gamma'}{\Gamma'^2 + \Omega_\mu'^2} + \frac{e^{-\Gamma'\tau_1}\Gamma_p(\Gamma'\cos\Omega_\mu'\tau_1 - \Omega_\mu'\sin\Omega_\mu'\tau_1)}{\Gamma'^2 + \Omega_\mu'^2},$$

$$\delta_{12}^i(z, \tau_1) = +\frac{\Gamma_p\Omega_\mu'}{\Gamma'^2 + \Omega_\mu'^2} - \frac{e^{-\Gamma'\tau_1}\Gamma_p(\Omega_\mu'\cos\Omega_\mu'\tau_1 + \Gamma'\sin\Omega_\mu'\tau_1)}{\Gamma'^2 + \Omega_\mu'^2}, \tag{23}$$

$$\frac{\partial\Gamma_p(z)}{\partial z} = -\alpha\frac{\Gamma_p(z)}{\Gamma^*}\left[1 + \frac{2}{2I+1}\delta_{12}^r(z, \tau_1)\right].$$

With the boundary condition $\Gamma_p(z=0) = \Gamma_{p0}$, the numerical solution of Eqs. (23) yields the atomic coherence at the end of the first Λ pulse in each point of the cell.

As in the optically thin case, the atoms evolve freely for a time T [according to the free evolution matrix, Eq. (10)] so that we have the coherence at $\tau_1 + T$ for any z:

$$\delta_{12}^r(z, \tau_1 + T) = e^{-\gamma_2 T}[\cos\Omega_\mu T \, \delta_{12}^r(z, \tau_1) + \sin\Omega_\mu T \, \delta_{12}^i(z, \tau_1)],$$

$$\delta_{12}^i(z, \tau_1 + T) = e^{-\gamma_2 T}[-\sin\Omega_\mu T \, \delta_{12}^r(z, \tau_1) + \cos\Omega_\mu T \, \delta_{12}^i(z, \tau_1)]. \tag{24}$$

Later, a second Λ pulse of duration τ_2 detects the clock transition. We then specify the first equation of Eqs. (22) for the detection pulse, using Eqs. (24) as initial condition; we find

$$
\delta_{12}^r(z, \tau_1 + T + \tau_2) = -\frac{\Gamma_p \Gamma'}{\Gamma'^2 + \Omega_\mu'^2} + e^{-\Gamma' \tau_2}\left[\delta_{12}^r(z, \tau_1 + T) + \frac{\Gamma' \Gamma_p}{\Gamma'^2 + \Omega_\mu'^2}\right]\cos \Omega_\mu' \tau_2
$$

$$
+ e^{-\Gamma' \tau_2}\left[\delta_{12}^i(z, \tau_1 + T) - \frac{\Omega_\mu' \Gamma_p}{\Gamma'^2 + \Omega_\mu'^2}\right]\sin \Omega_\mu' \tau_2,
$$

$$
\delta_{12}^i(z, \tau_1 + T + \tau_2) = \frac{\Gamma_p \Omega_\mu'}{\Gamma'^2 + \Omega_\mu'^2} + e^{-\Gamma' \tau_2}\left[\delta_{12}^i(z, \tau_1 + T) - \frac{\Omega_\mu' \Gamma_p}{\Gamma'^2 + \Omega_\mu'^2}\right]\cos \Omega_\mu' \tau_2
$$

$$
- e^{-\Gamma' \tau_2}\left[\delta_{12}^r(z, \tau_1 + T) + \frac{\Gamma' \Gamma_p}{\Gamma'^2 + \Omega_\mu'^2}\right]\sin \Omega_\mu' \tau_2. \tag{25}
$$

We are interested in the real part of the coherence, so that the final equation we have to solve is

$$
\frac{\partial \Gamma_p^{\text{det}}(z)}{\partial z} = -\alpha \frac{\Gamma_p^{\text{det}}(z)}{\Gamma^*}\left\{1 + \frac{2}{2I+1}\delta_{12}^r(z, \tau_1 + T + \tau_2)\right\}, \tag{26}
$$

where Γ_p^{det} is the pumping rate associated to the detection Λ pulse. Indeed, the detection of the clock transition is supposed to be performed via the transmission signal at the output of the cell, so it is proportional to Γ_p^{det} evaluated at $z = L$, L being the cell length. We point out that since in the experiments the pumping and the detection pulse amplitudes are the same we will assume $\Gamma_p(z = 0) = \Gamma_p^{\text{det}}(z = 0) = \Gamma_{p0}$.

As examples, Figs. 5 and 6 report Ramsey fringes as a result of the numerical solution of the previous equation for a ^{133}Cs cell at 40 °C and for a ^{87}Rb cell at 50 °C, respectively. The laser pumping rate Γ_{p0} is set equal to 8000 s^{-1} for the ^{133}Cs simulation, corresponding to 140 μW/cm^2, and to 10 000 s^{-1} (230 μW/cm^2) for the ^{87}Rb cell. In both cases, we considered the D_1 optical line.

In Figs. 5 and 6 and in all the simulations throughout the paper, we consider a ^{133}Cs cell with 25 Torr of N$_2$, and the corresponding homogeneous broadening due to buffer gas collisions is $\Gamma_{\text{BG}} \approx 2\pi \times 490$ MHz. The Doppler broadening evaluated for the D_1 line in a ^{133}Cs vapor cell at 40 °C turns out to be $\Gamma_D \approx 2\pi \times 370$ MHz; for simplicity we assume that

Γ_D does not change significantly in the range of temperatures of interest for this paper. For the Rb cell we consider a 25-Torr buffer gas mixture Ar + N$_2$ in the pressure ratio 1.6; an analogous evaluation of Γ_{BG} and Γ_D has been done for the ^{87}Rb cell.

Relaxation rates for ground-state population and coherence are evaluated according to the cell size, buffer gas content, and cell temperature [44].

B. Contrast and linewidth of the central Raman-Ramsey fringe

For frequency standards applications, it is interesting to evaluate the contrast and the linewidth of the central Ramsey fringe in different experimental conditions [45]. In effect, these two parameters play a role to determine the clock short-term frequency stability and it can be convenient for a given cell to evaluate the temperature, and then the atomic density, which maximizes their ratio. Contrast and linewidth have been then calculated at different temperatures, taking into account that—in addition to cell size, buffer gas content, and pressure—the ground-state relaxation rate γ_2 depends also on temperature through the spin-exchange contribution [44].

Figure 7 refers to the central Ramsey fringe linewidth for the same ^{133}Cs and ^{87}Rb cells previously considered. For convenience, we keep the same Ramsey time $T = 3.5$ ms in both cases. Two regimes can be identified as the optical
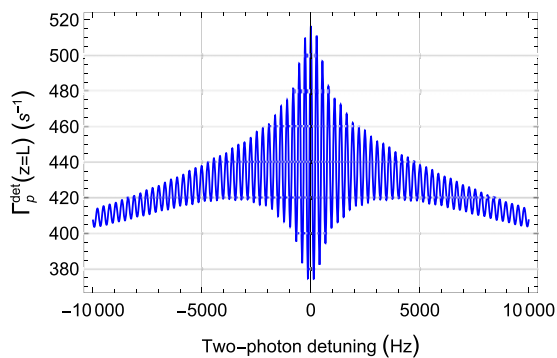

FIG. 5. Calculated Ramsey fringes for a cell containing ^{133}Cs and 25 Torr of N$_2$; $\Gamma_{p0} = 8000$ s^{-1}, cell temperature 35 °C; $\tau_1 = 1$ ms; $T = 3.5$ ms; $\tau_2 = 50\,\mu$s. Cell length $L = 2$ cm; radius $R = 1$ cm.
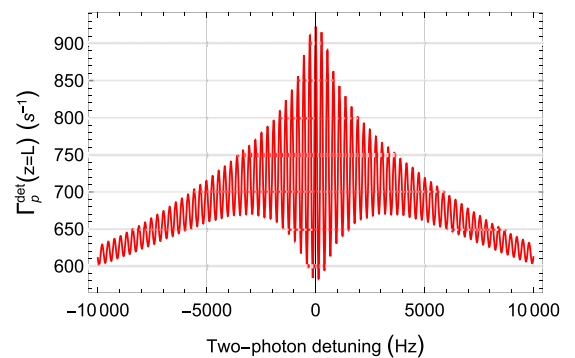

FIG. 6. Calculated Ramsey fringes for a cell containing ^{87}Rb and 25 Torr of Ar + N$_2$ in the pressure ratio 1.6; $\Gamma_{p0} = 10\,000$ s^{-1}, cell temperature 50 °C; $\tau_1 = 1$ ms; $T = 3.5$ ms; $\tau_2 = 50\,\mu$s. Cell length $L = 2$ cm; radius $R = 1$ cm.
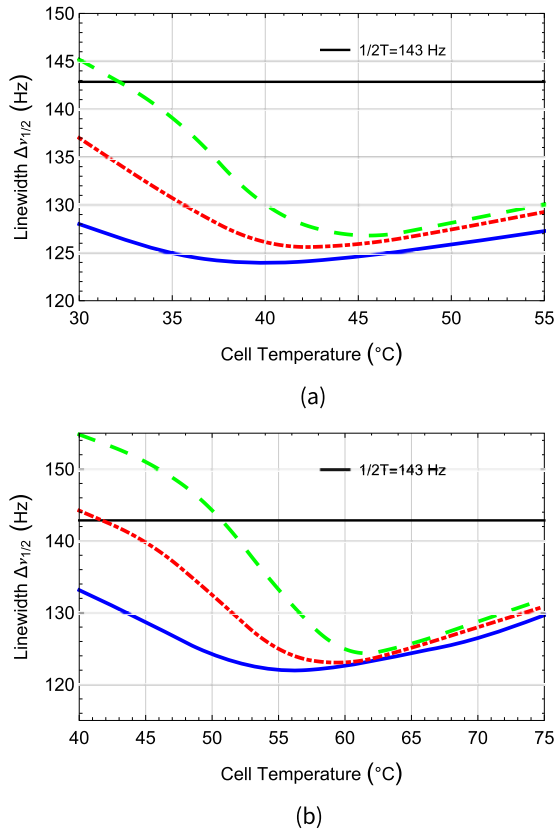
(a)

(b)

FIG. 7. Linewidth of the central Ramsey fringe for the same Cs (a) and Rb (b) cells considered in Figs. 5 and 6. The straight line is the $1/2T$ value; $t_p = 1$ ms; $T = 3.5$ ms; $\tau_2 = 50\,\mu$s. Continuous line, $\Gamma_{p0} = 3000$ s^{-1}; dash-dotted line, $\Gamma_{p0} = 10\,000$ s^{-1}; dashed line, $\Gamma_{p0} = 30\,000$ s^{-1}.

(a)

(b)

FIG. 8. Linewidth of the central Ramsey fringe as a function of the laser pumping rate for different values of the detection time τ_2. (a) Cs cell with the same buffer gas content and pressure of Fig. 5 at 30 °C. (b) Rb cell with the same buffer gas content and pressure of Fig. 6 at 40 °C. The straight line is the $1/2T$ value; $t_p = 1$ ms; $T = 3.5$ ms. Continuous line, $\tau_2 = 5\,\mu$s; dash-dotted line, $\tau_2 = 20\,\mu$s; dashed line, $\tau_2 = 50\,\mu$s.

thickness of the atomic medium is increased. First, we observe a decrease of the linewidth. This density-dependent spectral narrowing phenomenon is well known in coherently prepared atomic media and has been described in several works [46,47]. Basically, in the high-density limit, only spectral components which are very close to the center of the transparency window are transmitted. These narrowing effects have been observed in continuously operated experiments. Here we show that density narrowing takes place in the pulsed regime as well, affecting both the Rabi and the central Ramsey fringe. After reaching a minimum at a certain temperature, a broadening regime is predicted where the narrowing is compensated and eventually overcome by the increase of γ_2, similarly to what happens in continuous CPT.

The narrowing behavior depicted in Fig. 7 has been experimentally observed for a Cs cell in [38,39]. The high-temperature regime where the linewidth broadening occurs has not been investigated in those works.

As reported in the previous section for the optically thin medium, the detection time plays a role to determine the linewidth of the central Ramsey fringe. In this regard, it is convenient to consider the linewidth versus Γ_{p0} in the low-density regime where the narrowing phenomenon previously described barely impacts on the detection-time-dependent effects we are interested in. The results are reported in Fig. 8.
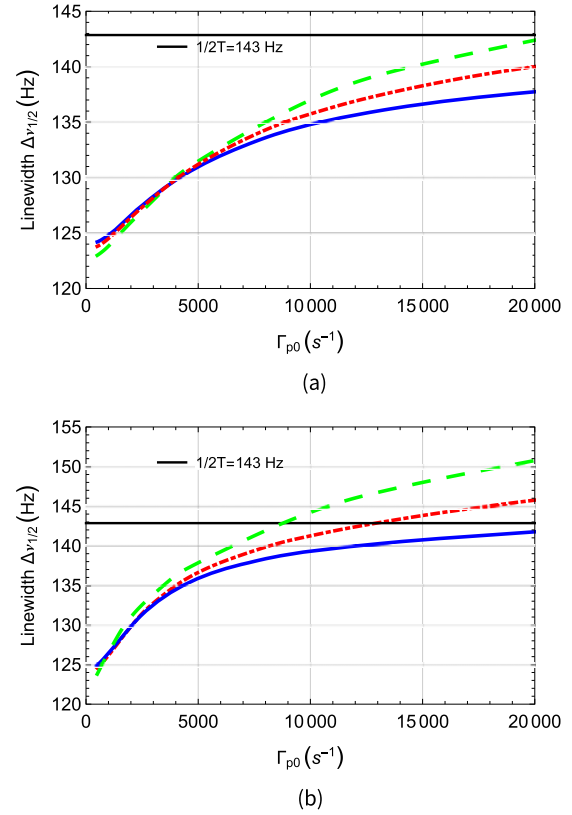
We observe that an increase of τ_2 enhances the laser power broadening both in Cs and in Rb. In Rb, the linewidth may even overcome the expected $1/2T$ value, as already observed for the optically thin medium. The reason for this behavior is that as the detection time is increased the circular functions containing τ_2 [see, for example, Eq. (13)] cannot be neglected anymore and contribute in a significant way to determine the linewidth (and also the shift as shown later on) of the resonance signal.

The linewidth can be also characterized in terms of its dependence on the laser intensity for different temperatures of the atomic vapor, as shown in Fig. 9. High-temperature regimes enhance the coherence properties of the atomic medium and the power broadening is compensated by a line narrowing for increasing laser pumping rates. Definitely, the linewidth becomes nearly insensitive to Γ_{p0}. We point out that a similar behavior is typical of coherently prepared media and has been already observed in the CPT maser under continuous operation and in high atomic density conditions [48].

As discussed in [38], it might not be surprising that the central fringe linewidth is narrower than $1/2T$. Indeed, in a common Ramsey interaction scheme where two microwave pulses are separated by a time T, the linewidth of the central fringe is $1/2T$ only in the limit of perfectly sharp microwave
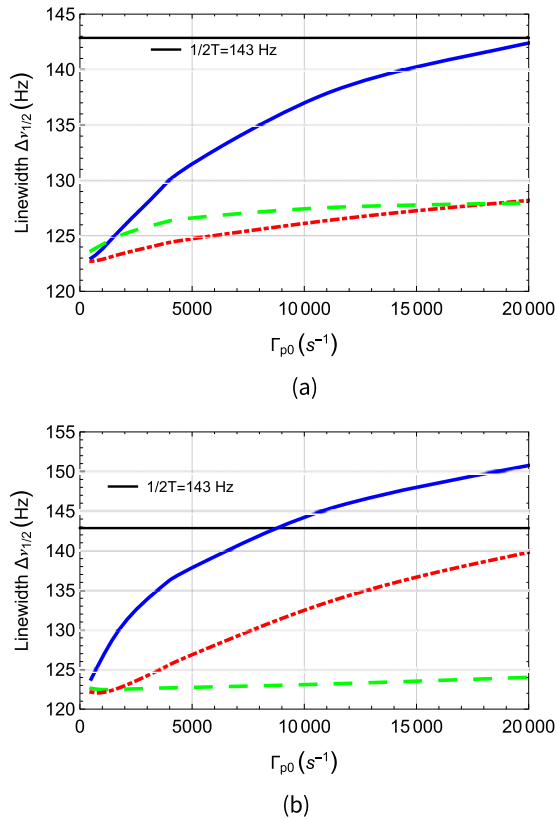
(a)

(b)

FIG. 9. Linewidth of the central Ramsey fringe of Raman-Ramsey resonances vs the laser pumping rate. The straight line is the $1/2T$ value; $\tau_1 = 1$ ms; $T = 3.5$ ms; $\tau_2 = 50\,\mu$s. (a) Cs cell: continuous line, 30 °C; dash-dotted line, 40 °C; dashed line, 50 °C. (b) Rb cell: continuous line, 40 °C; dash-dotted line, 50 °C; dashed line, 60 °C.
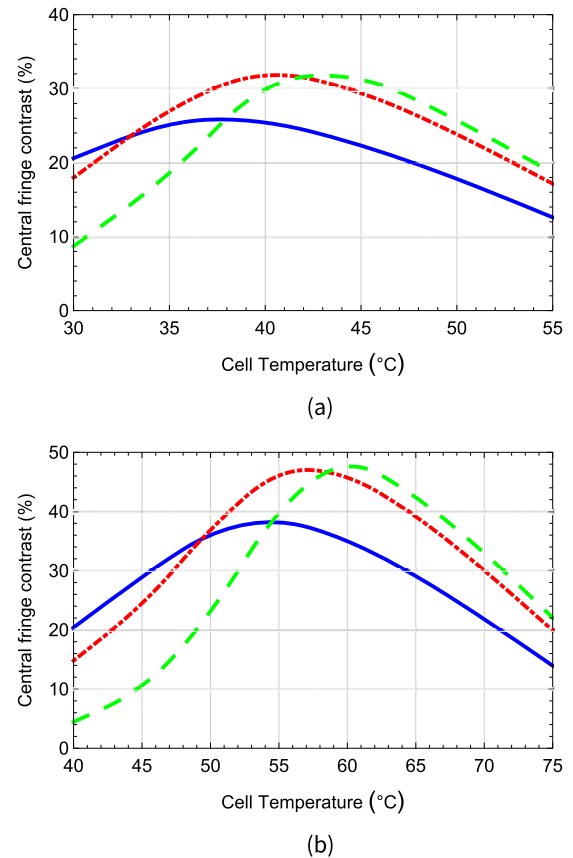

(a)

(b)

FIG. 10. Contrast of the central fringe of Raman-Ramsey resonances for the same Cs (a) and Rb (b) cells considered in Figs. 5 and 6; $\tau_1 = 1$ ms; $T = 3.5$ ms; $\tau_2 = 50\,\mu$s. Continuous line, $\Gamma_{p0} = 3000$ s^{-1}; dash-dotted line, $\Gamma_{p0} = 10\,000$ s^{-1}; dashed line, $\Gamma_{p0} = 30\,000$ s^{-1}.

pulses. For a finite duration t_1 of the microwave pulses, the linewidth turns out to be $\frac{1}{2(T+4t_1/\pi)}$ [49]. A similar argument might be also applied to the Raman-Ramsey approach. However, what is unexpected is that in a Ramsey-like scheme the linewidth exhibits a significant dependence on the detection time, the vapor temperature, and the laser intensity. The physical reason behind this behavior is that, even in the pulsed regime, the CPT interaction always involves three levels: the two clock levels and the excited state. Optical coherences are excited and they make the clock signal linewidth sensitive to a number of parameters, including vapor temperature and laser intensity.

In Fig. 10 we report on the contrast of the central Ramsey fringe as a function of temperature for different laser pumping rates. We notice that the temperature which maximizes the contrast is very close to that minimizing the linewidth, as already observed in [38].

A comparison between Cs and Rb can be done with caution. Even if the behaviors depicted in Figs. 7, 9, and 10 have been obtained for the same Ramsey time and pumping rate, the other cell parameters are different, including relaxation rates and absorption coefficients. Most importantly, according to the respective vapor pressure laws, Rb and Cs atomic densities can significantly differ at equal temperature, especially in the high-temperature regimes. However, to give an insight

into the results of the previous figures, we observe that due to its lower nuclear spin ^{87}Rb approaches the situation of an ideal three-level system better than ^{133}Cs. This means that at equal atomic densities in Rb there are more atoms in the two clock levels, and therefore coherent phenomena, like density narrowing effects, are expected to be more pronounced. For the same reason, contrasts for Rb are in general larger than in Cs.

C. Light shift in an optically thick vapor

Light shift in Raman-Ramsey resonances has been the subject of several recent works [50,51] and has been also studied in a cold-atom clock [52–54]. In this subsection, we assess light shift in an optically thick hot vapor.

Figure 11 reports the calculated light shift versus the laser pumping rate for different cell temperatures. As for the optically thin medium, the behavior can be explained in terms of a Rabi pulling effect, for small laser pumping rates, and a detection-time-dependent linear light shift when Γ_{p0} is increased. This linear behavior of the light shift has been already observed in Cs experiments for a cell working at 42 °C [51].

For both Cs and Rb cells, the conversion of laser intensity fluctuations to the clock frequency can benefit from
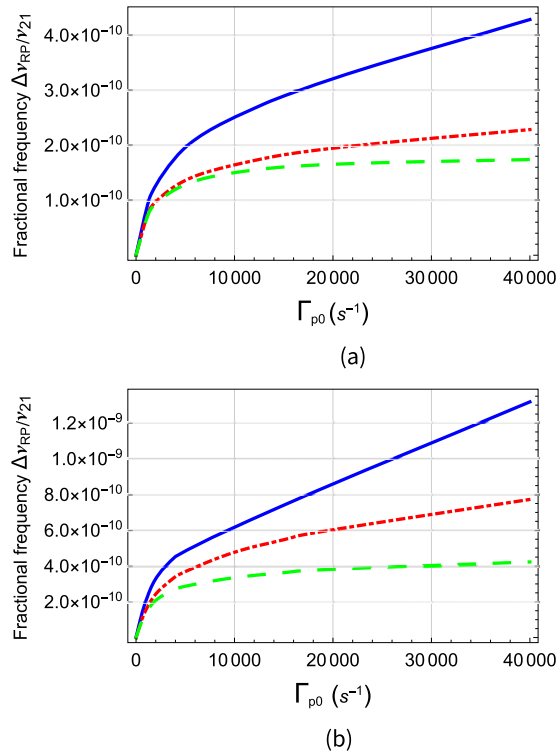
FIG. 11. Fractional light shift of the central fringe of Raman-Ramsey resonances vs the laser pumping rate; $\tau_1 = 1$ ms; $T = 3.5$ ms; $\tau_2 = 50 \,\mu$s. (a) Cs cell: continuous line, 30 °C; dash-dotted line, 40 °C; dashed line, 50 °C. (b) Rb cell: continuous line, 40 °C; dash-dotted line, 50 °C; dashed line, 60 °C.

high-temperature regimes. For the Cs cell, the conversion coefficient around $\Gamma_{p0} = 20\,000$ s^{-1} is 1.3×10^{-12}/% at a temperature of 30 °C; it reduces to 8.6×10^{-14}/% at a temperature of 50 °C, a value comparable to that of better performing vapor cell clocks. Similarly, for the Rb cell, the conversion factor decreases from 1.3×10^{-12} to 6.8×10^{-13}/% when the temperature is raised from 40 to 60 °C.

IV. DISCUSSION AND CONCLUSIONS

The main purpose of this paper was to give physical insight into light shift in pulsed CPT frequency standards and to provide a theoretical framework predicting the main features (linewidth and contrast) of dark resonances when observed in an optically thick vapor.

Pulsing the different operation phases of vapor cell clocks has been demonstrated to be very effective to reduce light shift and to improve their frequency stability performances. In this regard, pulsed CPT standards exhibit better performances than continuously operated CPT clocks, even though light shift remains one of the main sources of frequency instability in the medium to long term. Light shift should be negligible when the resonance is detected in the pulsed regime: the atoms make the clock transition in the dark and no transfer of laser instabilities to the clock levels is expected. However, even if CPT coherently superimposes the two ground-state levels, this coherence turns out to be coupled to the excited state. The pulsed technique mitigates the interplay between

microwave and optical coherences; nevertheless, the Rabi interaction keeps memory of the laser field and induces a pulling effect on the central Ramsey fringe: basically, with reference to Eq. (16), the Rabi profile is centered in $\Omega_\mu = \omega_R^2/2\omega_{21}$, whereas the Ramsey fringe is centered in $\Omega_\mu = 0$. In other words, the Rabi interaction is the mechanism through which laser intensity instabilities are transferred to the clock signal.

To be noticed is the difference with the pulsed optical pumping (POP) approach [55,56] where the laser is used to solely invert the ground-state population, the coherence being generated by a microwave signal. In this case light shift is truly almost negligible. At any rate, the theory here reported shows that it is possible to reduce the transfer of laser intensity fluctuations to pulsed CPT resonances by increasing the laser intensity itself.

We analyzed the effect of the atomic density on the contrast and on the linewidth of the central Ramsey fringe. Two different behaviors have been identified for the linewidth: a density narrowing followed by a line broadening above a certain temperature.

The theory well describes the density narrowing and the contrast as observed in Cs vapors. Raman-Ramsey resonances have been also analyzed in Rb experiments [57–59] that can therefore provide an additional test bench of the theory.

We also pointed out the role played by the detection time to determine the linewidth and the shift of the clock signal. Specifically, fluctuations of the laser intensity affect the clock transition through a term proportional to τ_2, as also reported in [54] for a cold atom sample under CPT. This detection-time-dependent light shift is inherent to the detection process and may be an important cause of frequency instability in the medium- to long-term period. On the other hand, a long detection time yields a good signal-to-noise ratio and then a good short-term stability. Therefore, in experiments a tradeoff between these two situations must be found.

Further refinements of the theory are workable. A multi-level approach, similar to that reported in [60,61], including the whole ground-state manifold might lead to an even closer matching between theory and experiments.

Other phenomena may contribute to affect the linewidth and the line shape of pulsed CPT resonances. For example, also for an optically thin medium, the shape of continuously operated CPT resonances is sensitive to transverse intensity distribution of the light beam [62,63]. Moreover, in a cell with buffer gas, it is well known that the CPT resonance can experience a diffusion-induced spectral narrowing [64]. These phenomena may play a role also in pulsed operation; however, they are not considered in this paper.

As discussed in the previous section, it is not surprising that the linewidth of the central Ramsey fringe is narrower than $1/2T$, but its significant dependence on temperature and on laser intensity could be unexpected. Again, a comparison with the POP clock can shed some light on this behavior. In the case of the POP clock, after the optical pumping phase the atoms are interrogated by a couple of microwave pulses followed by a laser pulse which probes the number of atoms making the clock transition. This makes the central Ramsey fringe very robust against the variation of several parameters, including laser and microwave powers, and temperature. Only

for very high vapor temperatures, nonlinear phenomena affecting the clock linewidth have been observed [49]. In the pulsed CPT, the atomic population cannot be probed, being almost negligible. The information about the clock transition is contained in the ground-state coherence that, as previously mentioned, is coupled to the excited state. In other words, the CPT phenomenon, even in the pulsed regime, always involves three atomic levels and this makes CPT resonances more susceptible to the variations of the physical parameters.

However, due to its intrinsic simplicity, the CPT technique remains very attractive in view of implementing particularly compact devices. The theoretical analysis reported here is of interest in this regard since it can predict several important parameters, like contrast and linewidth, that have an impact on the clock frequency stability. Also, the theory presented here is absolutely general and can be applied, as well, to study dark resonances in optically thick media observed in microcells.

[1] R. G. Brewer and E. L. Hahn, Phys. Rev. A **11**, 1641 (1975).

[2] R. M. Whitley and C. R. Stroud, Phys. Rev. A **14**, 1498 (1976).

[3] V. Shah and J. Kitching, Advances in coherent population trapping for atomic clocks, in *Advances in Atomic, Molecular, and Optical Physics*, edited by E. Arimondo, P. Berman, and C. Chin (Elsevier, 2010), Vol. 59, pp. 21–74.

[4] J. Vanier, Appl. Phys. B **81**, 421 (2005).

[5] E. Breschi, Z. D. Grujić, P. Knowles, and W. A, Appl. Phys. Lett. **104**, 023501 (2014).

[6] M. Stähler, S. Knappe, C. Affolderbach, W. Kemp, and R. Wynands, Europhys. Lett. **54**, 323 (2001).

[7] A. Nagel, L. Graf, A. Naumov, E. Mariotti, V. Biancalana, D. Meschede, and R. Wynands, Europhys. Lett. **44**, 31 (1998).

[8] M. M. Kash, V. A. Sautenkov, A. S. Zibrov, L. Hollberg, G. R. Welch, M. D. Lukin, Y. Rostovtsev, E. S. Fry, and M. O. Scully, Phys. Rev. Lett. **82**, 5229 (1999).

[9] M. Bajcsy, A. S. Zibrov, and M. D. Lukin, Nature (London) **426**, 638 (2003).

[10] A. Godone, F. Levi, and S. Micalizio, Phys. Rev. A **66**, 043804 (2002).

[11] A. Aspect, E. Arimondo, R. Kaiser, N. Vansteenkiste, and C. Cohen-Tannoudji, J. Opt. Soc. Am. B **6**, 2112 (1989).

[12] J. E. Thomas, P. R. Hemmer, S. Ezekiel, C. C. Leiby, R. H. Picard, and C. R. Willis, Phys. Rev. Lett. **48**, 867 (1982).

[13] P. R. Hemmer, S. Ezekiel, and C. C. Leiby, Opt. Lett. **8**, 440 (1983).

[14] P. R. Hemmer, M. S. Shahriar, H. Lamela-Rivera, S. P. Smith, B. E. Bernacki, and S. Ezekiel, J. Opt. Soc. Am. B **10**, 1326 (1993).

[15] N. Cyr, M. Tetu, and M. Breton, IEEE Trans. Instrum. Meas. **42**, 640 (1993).

[16] A. Godone, F. Levi, S. Micalizio, and C. Calosso, Phys. Rev. A **70**, 012508 (2004).

[17] J. Danet, M. Lours, S. Guérandel, and E. De Clercq, IEEE Trans. Ultrason. Ferroelect. Freq. Control **61**, 567 (2014).

[18] A. Godone, F. Levi, C. E. Calosso, and S. Micalizio, Riv. Nuovo Cimento **38**, 133 (2015).

[19] S. Knappe, R. Wynands, J. Kitching, H. G. Robinson, and L. Hollberg, J. Opt. Soc. Am. B **18**, 1545 (2001).

[20] E. E. Mikhailov, T. Horrom, N. Belcher, and I. Novikova, J. Opt. Soc. Am. B **27**, 417 (2010).

[21] J. Vanier, M. W. Levine, S. Kendig, D. Janssen, C. Everson, and M. J. Delaney, IEEE Trans. Instrum. Meas. **54**, 2531 (2005).

[22] M. Merimaa, T. Lindvall, I. Tittonen, and E. Ikonen, J. Opt. Soc. Am. B **20**, 273 (2003).

[23] H. S. Moon, S. E. Park, Y.-H. Park, L. Lee, and J. B. Kim, J. Opt. Soc. Am. B **23**, 2393 (2006).

[24] V. Gerginov, S. Knappe, V. Shah, P. D. D. Schwindt, L. Hollberg, and J. Kitching, J. Opt. Soc. Am. B **23**, 593 (2006).

[25] J. Kitching, Appl. Phys. Rev. **5**, 031302 (2018).

[26] R. Boudot, V. Maurice, C. Gorecki, and E. de Clercq, J. Opt. Soc. Am. B **35**, 1004 (2018).

[27] F.-X. Esnault, E. Blanshan, E. N. Ivanov, R. E. Scholten, J. Kitching, and E. A. Donley, Phys. Rev. A **88**, 042120 (2013).

[28] J. Vanier and C. Mandache, Appl. Phys. B **87**, 565 (2007).

[29] T. Bandi, C. Affolderbach, C. Stefanucci, F. Merli, A. K. Skrivervik, and G. Mileti, IEEE Trans. Ultrason. Ferroelectr. Freq. Control **61**, 1769 (2014).

[30] A. Nagel, S. Brandt, D. Meschede, and R. Wynands, Europhys. Lett. **48**, 385 (1999).

[31] V. Shah, V. Gerginov, P. D. D. Schwindt, S. Knappe, L. Hollberg, and J. Kitching, Appl. Phys. Lett. **89**, 151124 (2006).

[32] M. Zhu and L. S. Cutler, in *Proceedings of the 32nd Precise Time and Time Interval (PTTI) Meeting*, 2000, pp. 311–324.

[33] F. Levi, A. Godone, and J. Vanier, IEEE Trans. Ultrason. Ferroelectr. Freq. Control **47**, 466 (2000).

[34] P. R. Hemmer, M. S. Shahriar, V. D. Natoli, and S. Ezekiel, J. Opt. Soc. Am. B **6**, 1519 (1989).

[35] S. M. Shahriar, P. R. Hemmer, D. P. Katz, A. Lee, and M. G. Prentiss, Phys. Rev. A **55**, 2272 (1997).

[36] T. Zanon, S. Guerandel, E. de Clercq, D. Holleville, N. Dimarcq, and A. Clairon, Phys. Rev. Lett. **94**, 193002 (2005).

[37] M. Abdel Hafiz, G. Coget, M. Petersen, C. E. Calosso, S. Guérandel, E. de Clercq, and R. Boudot, Appl. Phys. Lett. **112**, 244102 (2018).

[38] M. Abdel Hafiz, G. Coget, P. Yun, S. Guérandel, E. de Clercq, and R. Boudot, J. Appl. Phys. **121**, 104903 (2017).

[39] P. Yun, F. Tricot, C. E. Calosso, S. Micalizio, B. François, R. Boudot, S. Guérandel, and E. de Clercq, Phys. Rev. Applied **7**, 014018 (2017).

[40] M. D. Rotondaro and G. P. Perram, J. Quant. Spectrosc. Radiat. Transf. **57**, 497 (1997).

[41] A. Godone, S. Micalizio, and F. Levi, Phys. Rev. A **70**, 023409 (2004).

[42] L. Allen and J. H. Eberly, *Optical Resonance and Two-Level Atoms* (Dover, New York, 1987).

[43] A. Godone, F. Levi, S. Micalizio, and J. Vanier, Eur. Phys. J. D **18**, 5 (2002).

[44] J. Vanier and C. Audoin, *The Quantum Physics of Atomic Frequency Standards* (Hilger, London, 1989).

[45] X. Liu, J.-M. Mérolla, S. Guérandel, E. de Clercq, and R. Boudot, Opt. Express **21**, 12451 (2013).

[46] M. D. Lukin, M. Fleischhauer, A. S. Zibrov, H. G. Robinson, V. L. Velichansky, L. Hollberg, and M. O. Scully, Phys. Rev. Lett. **79**, 2959 (1997).

[47] G. Wang, Y.-S. Wang, E. K. Huang, W. Hung, K.-L. Chao, P.-Y. Wu, Y.-S. Chen, and I. A. Yu., Sci. Rep **8**, 7959 (2018).

[48] A. Godone, F. Levi, and S. Micalizio, Phys. Rev. A **65**, 031804(R) (2002).

[49] S. Micalizio, C. E. Calosso, F. Levi, and A. Godone, Phys. Rev. A **88**, 033401 (2013).

[50] G. S. Pati, Z. Warren, N. Yu, and M. S. Shahriar, J. Opt. Soc. Am. B **32**, 388 (2015).

[51] Y. Yano, W. Gao, S. Goka, and M. Kajita, Phys. Rev. A **90**, 013826 (2014).

[52] E. Blanshan, S. M. Rochester, E. A. Donley, and J. Kitching, Phys. Rev. A **91**, 041401(R) (2015).

[53] K. Barantsev, G. Voloshin, A. Litvinov, and E. Popov, EPJ Web Conf. **190**, 04003 (2018).

[54] J. W. Pollock, V. I. Yudin, M. Shuker, M. Y. Basalaev, A. V. Taichenachev, X. Liu, J. Kitching, and E. A. Donley, Phys. Rev. A **98**, 053424 (2018).

[55] S. Micalizio, C. E. Calosso, A. Godone, and F. Levi, Metrologia **49**, 425 (2012).

[56] S. Kang, M. Gharavipour, C. Affolderbach, F. Gruet, and G. Mileti, J. Appl. Phys. **117**, 104510 (2015).

[57] P. Yun, Y. Zhang, G. Liu, W. Deng, L. You, and S. Gu, Europhys. Lett. **97**, 63004 (2012).

[58] G. Pati, K. Salit, R. Tripathi, and M. Shahriar, Opt. Commun. **281**, 4676 (2008).

[59] S. N. Nikolić, M. Radonjić, N. M. Lučić, A. J. Krmpot, and B. M. Jelenković, J. Phys. B **48**, 045501 (2015).

[60] S. Micalizio, A. Godone, F. Levi, and C. Calosso, Phys. Rev. A **79**, 013403 (2009).

[61] A. V. Taĭchenachev, V. I. Yudin, R. Wynands, M. Stähler, J. Kitching, and L. Hollberg, Phys. Rev. A **67**, 033810 (2003).

[62] F. Levi, A. Godone, J. Vanier, S. Micalizio, and G. Modugno, Eur. Phys. J. D **12**, 53 (2000).

[63] A. V. Taĭchenachev, A. M. Tumaikin, V. I. Yudin, M. Stähler, R. Wynands, J. Kitching, and L. Hollberg, Phys. Rev. A **69**, 024501 (2004).

[64] Y. Xiao, I. Novikova, D. F. Phillips, and R. L. Walsworth, Phys. Rev. Lett. **96**, 043601 (2006).